IEEE Access
Multidisciplinary | Rapid Review | Open Access Journal

Received December 21, 2018, accepted January 3, 2019, date of publication January 21, 2019, date of current version February 6, 2019.

Digital Object Identifier 10.1109/ACCESS.2019.2893451

Experimental Multi-User Visible Light Communication Attocell Using Multiband Carrierless Amplitude and Phase Modulation

MOUNIR MOHAMMEDI MERAH, HONGYU GUAN, AND LUC CHASSAGNE, (Member, IEEE)
Laboratoire d'Ingénierie des Systèmes de Versailles, Université de Versailles Saint-Quentin, University of Paris-Saclay, 78140 Versailles, France

Corresponding author: Hongyu Guan (hongyu.guan@uvsq.fr)

This work was supported in part by the French Government and in part by the startup OLEDCOMM through the UVSQ-OLEDCOMM industrial partnership.

ABSTRACT Multi-band carrierless amplitude and phase modulation and subcarrier multiplexing (SCM) are combined to produce a novel multi-users access scheme for visible light communications (VLC). To demonstrate this scheme, an experimental and realistic scenario is set-up by using a low-cost commercial office white light-emitting diode (LED) downlight. Furthermore, subcarrier spacings are added to reduce the inter-channel interferences and the parameters of the pulse shaping filters are optimized. The distance between the transmitter and the receiver is fixed at 2.15 m. After the optimization, the experiment setup achieves a spectral efficiency of 5.08 b/s/Hz after subcarrier spacing and with very light post-processing. A total of 20 users can be provided with the multi-users access scheme with a sum data rate of 162.5 Mb/s. The receiving attocell is measured at 4.56 m^2. To the best of our knowledge, the resulting work presents the highest range, and one of the highest spectral efficiencies for a phosphorous white LED (ph-LED)-based VLC system, thanks to subcarrier spacing. With SCM, it is also the first ph-LED-based VLC multi-users system.

INDEX TERMS Multi-band CAP, subcarrier multiplexing, multi-user access, visible light communication, white LED, subcarrier spacing, attocell.

I. INTRODUCTION

Visible Light Communications (VLC) known as Light-Fidelity (Li-Fi) is one of the most promising wireless communication techniques for 5G and beyond [1], [2]. The approach is to operate visible light between the 375 nm and 780 nm wavelengths to transmit data by applying an intensity modulation. The technique promises to find a solution to many of the ongoing wireless communication problems such as the radio-frequency bandwidth saturation and the increasing mobile data demand. As such, many researches are geared towards the exploration of the technology. Most are aimed at increasing the data rate. Indeed, the throughput is constrained by hardware inherent bandwidth limitations from the LED emitter. A second topic is the addition of a multi-users layer to VLC systems. Various types of Multiple Access Control (MAC) schemes exist and need to be considered when setting up an attocell. Other trending topics include vehicle communication [3], and positioning [4]. In this paper, we focus on the first two topics.

A. LED LIGHTING DEVICE

The first key barrier is the limited modulation bandwidth of the lighting devices. The most common technology is white light-emitting diodes (LED) in indoor scenarios. They primarily utilize two types: based on trichromatic Red Green Blue (RGB) LED, or based on a blue-chip LED with a yellow phosphor layer. Presently, indoor places use blue-chip based LEDs because the implementation of RGB LEDs demands more advanced drivers and has a higher implementation cost [5]. The LED downlight is the lighting solution of choice in indoor places such as homes, offices, malls or museums. Therefore, a commercial phosphorous-type LED downlight is used throughout the paper for a more realistic scenario.

B. MODULATION

The highest measured data rate for a VLC system using a single phosphor-based white LED (ph-LED) is 2.32 Gbit/s, as reported in [6]. The spectral efficiency is 5.155 b/s/Hz, the highest in these conditions. On top of using orthogonal frequency division multiplexing (OFDM), a two-stage equalizer and a maximum ratio combining (MRC) algorithm on two receivers are used. A 4.62 b/s/Hz VLC system using a ph-LED is presented in [7], and uses a power exponential software equalizer as well as two receivers with a combining algorithm. The common problem is that Ph-LEDs can only be modulated to a few MHz due to the phosphor layer. This explains why heavily complex techniques are used to increase the spectral efficiency. The preferred method is the use of high spectral efficiency modulation formats to better exploit the bandwidth of the LEDs. OFDM and its variants are the more explored modulation schemes [8], and uses fast Fourier transform (FFT) and inverse FFT (IFFT). Carrierless Amplitude and Phase (CAP) modulation is a similar scheme, but uses pairs of orthogonal pulse shaping filters instead of IFFT/FFT. It is a variant of quadrature amplitude modulation (QAM) where two pulse amplitude modulated signals are filtered with two filters forming a Hilbert pair. Its performances in spectral efficiency are similar to OFDM, but it has lower peak to average power ratio, as shown in [9]. Our attention is directed to multiband CAP (m-CAP), bringing conventional CAP into a multi-carrier format. It was first investigated in fiber optics with promising results, such as in [10]–[12]. It adds a multi-carrier component to CAP to reduce the sensitivity to non-flat channel response. In addition, an increase of the flexibility comes with the ability to select a modulation order for each subcarrier.

The exploration of the m-CAP modulation applied to VLC is in its early stages. A previous study includes a demonstration of the scheme with a 4.85 b/s/Hz spectral efficiency in [13]. However, it uses a GaN LED and did not aim to optimize the data rate. Other works also present the influence of the filter parameters in m-CAP [14], and the impact of the number of subcarriers and the effect of equalization [15]. The potential of m-CAP for high transfer speeds in VLC is associated with 4x4 imaging MIMO in [16]. The data rate reaches 249 Mb/s using LEDs with a 4 MHz bandwidth, 20 subcarriers and a 20 MHz signal at a range of one meter. As such, the spectral efficiency for each of the four imaged links achieves 3.11 b/s/Hz. The potential for multi-users is demonstrated first in [17]. The transmitter is an RGB LED with a 30 cm distance from the receiver. The spectral efficiency is 5.14 b/s/Hz per chip (450 Mb/s). Nine users are served, but heavy post-processing is needed with an advanced post-equalization method on top of the very limited distance. In [18], a red LED serves five users, but requires heavy post-processing involving a machine learning based nonlinear compensator.

With m-CAP, a high data rate can be achieved. However, the multi-users aspect is still missing, and it would be essential in any scenario involving a VLC system using a LED downlight. Indeed, it can be used in an office, a hospital, a mall or a museum. In every scenario, a multi-access component remains a key aspect.

C. MULTI-USER ACCESS

The focus of most research on multi-user access schemes is to decrease the amount of inter-user and inter-cell interferences. Indeed, attocell networking has been heavily studied. At the same time, experimentally implemented single attocell performances are less explored. X. Huang *et al.* worked on a combination of two OFDM schemes for attocell networking in [19]. Other similar attocell network literature includes the work presented by Ma *et al.* [20]. A coordination of multiple VLC attocells is performed through power line communication (PLC). Other examples include the works by Kazemi *et al.* [21], Alshaer and Haas [22], or Li and Zhang [23]. They all demonstrated the networking of multiple attocells using novel methods with various advantages. This paper focuses on the experimental performances of a single attocell. However, these two types of papers are complementary, as their demonstrations show the architecture of an attocell network while our production expands on the performance of individual access points.

Subsequently, very few works implement an experimental multi-users VLC system. Using multiband CAP a few experimental multi-access setup were realized in [17] and [18] as described in the previous subsection. However, results were acquired either at an unrealistic distance or with substantial post-processing. An orthogonal frequency-division multiple access (OFDMA) based system achieved a data rate of 13.6 Mb/s per user in [24]. It utilized a ph-LED at a 10 cm range, for two users. The distance is small enough to be considered unrealistic, and performance is limited. A Multi-Carrier Code Division Multiple Access (MC-CDMA) based demonstration reaches 47 Mb/s per user, for 16 users, as shown in [25]. It uses red LED and an avalanche photo-diode (APD) over 1.5 meters, but requires heavy post-processing with pre- and post-equalization and Walsh–Hadamard codes.

There are a considerable number of multi-user access schemes that have been investigated like Carrier Sense Multiple Access (CSMA), Time Division Multiple Access (TDMA), or CDMA. The latest research focus on optical space division multiple access (SDMA) which uses directional light beams oriented at the position of a user [26]. However, it requires complex transmitters with the ability to locate users and multiple narrow field-of-views (FOV) LEDs. Multi-user multiple-input multiple-output (MU-MIMO) is a complex MIMO technique where multiple LEDs are coordinated to provide for a number of users [27]. Nevertheless, it suffers from heavy computational complexity and power consumption. While these mentioned schemes are promising, their anticipated performances have yet to be experimentally proven in a realistic scenario.

Non-Orthogonal Multiple Access (NOMA) is another promising technology for 5G [28]. Power domain NOMA in VLC has been explored in [29], but requires a high SNR to perform optimally with multiple users. An experimental setup has been demonstrated by Lin *et al.* [30] where NOMA is combined with OFDM. It resulted in a system transmitting at 1.7 Mbaud with a signal bandwidth of 1.25 MHz. A ph-LED is used with two photodiodes representing 2 users and a distance of up to 30 cm. Another similar work is presented by Chen *et al.* [31]. Their proof of concept experiment attains a sum data rate of 45 Mb/s at a distance of 1 meter and a signal bandwidth of 15 MHz. While the performances are unimpressive, these demonstrations highlight power domain NOMA as an ideal candidate for capacity improvement in VLC systems. However, the potential of the scheme is yet to be realized, as concluded by both papers. To some extent, they represent a perspective as both our scheme and NOMA can be combined as explained in [30].

Consequently, the preferred scheme for our realistic scenario is subcarrier multiplexing (SCM). Indeed, it is a widely used technique in fiber optics [32]. However, our scenario uses a LED in an indoor room and not a laser. As a consequence, performances optimizations are needed to adapt the association with VLC.

D. OUR APPROACH

In this paper, the modulation m-CAP is associated with the multi-access scheme subcarrier multiplexing. The demonstration uses a realistic indoor scenario with low-complexity post-processing for multiple users. The distance between the transmitter and the user plane is set at 2.15 meters as it is the average ceiling to desk range in offices. The post-process utilizes very simple pre- and post-equalization schemes. The factor that allows us to improve the performances with moderate cost is subcarrier spacing. First introduced in our previous work in [33], this contribution is considerably expanded in this paper in three ways. The first is the expanded results with added realism of the experiment. Additionally, the process is performed on all subcarriers individually and not on groups of subbands. The second addition is the presence of intermediary results in the process which offers valuable details on the optimization process. The third addition is the extension on the multi-user ability of the scheme through the impact of the optimization on the cell size and the distance. This link between the results in data rate performances and the multi-user aspect is a significant contribution.

SCM offers an established way to provide for multiple users. Carrier aggregation [34] also adds flexibility. With the SCM scheme this allows for more subbands per user. As far as our knowledge goes, it is the first experimental demonstration of a commercial ph-LED downlight based VLC multi-users system with such a high number of users.

Fig. 1 shows the objective in spectral efficiency versus complexity level this works aims at. The complexity of an experimental VLC system is defined as the sum of the level of complexity on each part of the transmission chain. Table 1 details the level of complexity for each part. The references that were retained contain a VLC indoor experimental demonstration using a LED. Laser-based systems were included when relevant for the comparison. The redundant references were removed when the same setup is re-used through multiple papers from the same authors, keeping the most recent results. This figure is subjective and its interpretation remains at the discretion of every reader. However, it depicts a distinct vision of our approach relating the complexity of the scheme.

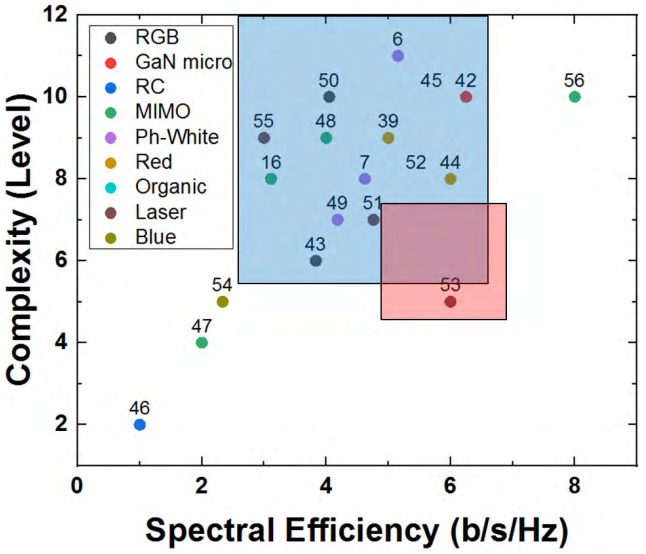

FIGURE 1. Estimation of the level of complexity of the VLC experimental setup versus the spectral efficiency. The blue area is the most explored, where the spectral efficiency is between 3 and 7 b/s/Hz and the estimated complexity is higher than 6. The red area is the objective aimed by our work, with a spectral efficiency around 5 and an estimated complexity around 6. References [51] and [53] are laser based experiment used as a comparison.

TABLE 1. Definition of the estimated level of complexity for a VLC experimental setup.

Transceiver bloc	Technology	Estimation of the level of complexity
Modulation and Demodulation	OOK, PAM or similar	+0
	CAP, GSSK	+2
	Multiband CAP, OFDM, FBMC	+3
	DFT-S OFDM	+4
Pre-equalization	None	+0
	Present	+2
Post-equalization	None	+0
	1-stage	+2
	Multi-stage, machine-learning	+3
Emitter technology	Single LED	+0
	LED Matrix	+2
	MIMO	+3

E. PAPER LAYOUT

Section 2 explains the principle of multi-users multi-band CAP (MU m-CAP). Section 3 describes the experimental setup and the white ph-LED downlight characteristics.

Section 4 presents the investigation on the optimization of spectral efficiency with subcarrier spacing. Section 5 depicts the resulting VLC multi-users attocell with its characteristics. Finally, the paper concludes with a summary of the study.

II. PRINCIPLE OF MULTI-USERS MULTI-BAND CAP

The principle of multi-band CAP (m-CAP) is to divide a conventional CAP signal into m independent subbands. Modulation order and optical power on each subcarrier can be tailored to its SNR. 1-CAP modulation is sensitive to non-flat frequency response like VLC channels. Multi-band CAP alleviates this drawback since dividing the signal into multiple subcarriers reduces the frequency length of each subband. Consequently, the frequency response for each band is more flat than the global response. Therefore, m-CAP is less prone to attenuation induced distortion than conventional CAP. Another advantage of multi-band CAP is the flexibility inherent to a multi-subcarrier modulation scheme. Each subcarrier can be affected a specific QAM modulation order and a distinct power level. This flexibility is used in OFDM to attain higher spectral efficiencies by assigning superior modulation order to the subbands with high SNR. The Bit Error Ratio (BER) is then optimized by adjusting the power of each subcarrier.

As opposed to OFDM, m-CAP uses FIR filters instead of IFFT/FFT. *m* represents the number of subcarrier. When increasing m the number of transmission filters increases by 2m. Since the square root raised cosine used is a finite impulse response (FIR) filter, the implementation cost would logically increase. However, the orthogonal pulse shaping pair filters become simpler to implement because each pair covers a smaller frequency band. Indeed, a sampling rate closer to the Nyquist rate can be used, which decreases the digital signal processing clock. On top of the fact that CAP does not use FFT, it makes CAP an ideal choice for a simple-to-implement high spectral efficiency modulation. This defining characteristic motivates the choice of this scheme over OFDM.

With multi-user m-CAP using SCM, the multiple subcarriers data streams correspond with multiple users. Each user data is contained in one or more subbands as illustrated on Fig. 2. For example, if two users are allocated using 4-CAP, two subcarriers per user or three to user 1 and only one to user 2 could be allocated. This ability to allocate various number of subbands to each user depends on the needs and channel state, making MU-m-CAP a very flexible multi-users access scheme. This is called carrier aggregation [34]. A user can be dynamically allocated more subcarriers than the others if it needs a data rate increase or if the quality of its signal decreases. Additionally, if m increases, this flexibility escalates as more subcarriers are available for each user.

The receiver needs to know the user-subcarriers allocation. A bidirectional link would add the ability to configure the distribution of subbands. VLC requires an amount of power to generate light that cannot be attained by mobile devices and is therefore not preferred. Also, interferences are created

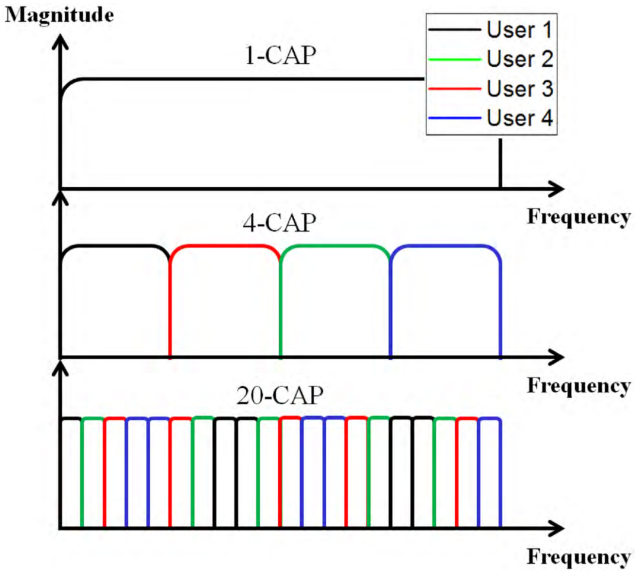

FIGURE 2. Ideal frequency responses and user allocation example in a 4-users scenario with SCM for conventional CAP (top), 4-CAP (middle) and 16-CAP (bottom). 1-CAP can only allocate one user when using SCM.

by the reflected light between the two channels. As a first alternative, radio-frequency (RF) is easy to use but requires the transceivers to work in two domains and cannot be used when electromagnetic interferences (EMI) need to be minimized. As a second alternative, retro-reflective transceivers reflect light to transmit data but the modulation speed is low [35]. However, efforts have been made to overcome this limitation [36] and the technology is promising for VLC. Finally, as suggested in [37], a near ultraviolet (UV) or near infrared (IR) up-link seems to be the most viable solution currently. Indeed, as shown by [38], range for an uplink option is approximately the same between the visible, near UV, and IR bands.

$$c_k = \{a_{k,1}, a_{k,2}, ..., a_{k,j}\} \tag{1}$$

In equation (1), each a $_{k,j}$ represents a subcarrier number j that is allocated to the user k. With $k \in [1{:}l]$ and $j \in [1{:}n]$, there can be up to l users and one user can have one to n subcarriers assigned. At the transmission, each of the k data streams d_k are divided into j streams of symbols corresponding to the j subcarriers assigned to that user. The m streams symbols are mapped on their corresponding $Ma_{k,j}$-QAM mapper, with $Ma_{k,j}$ designating the modulation order at the nth subcarrier. From now, each n corresponds to an assigned subcarrier $a_{k,j}$. The mapped symbols are then up-sampled and separated into their in-phase (real) and quadrature (imaginary) components. The m pairs of in-phase and quadrature components (I/Q) are then filtered with square root raised cosine filters at different frequencies depending on the subcarrier number. A_I^n and A_Q^n are defined as the up-sampled in-phase and quadrature M$_n$-QAM mapped symbols on the nth subcarrier. The overall sketch of the principle is illustrated in Fig. 3 (a).

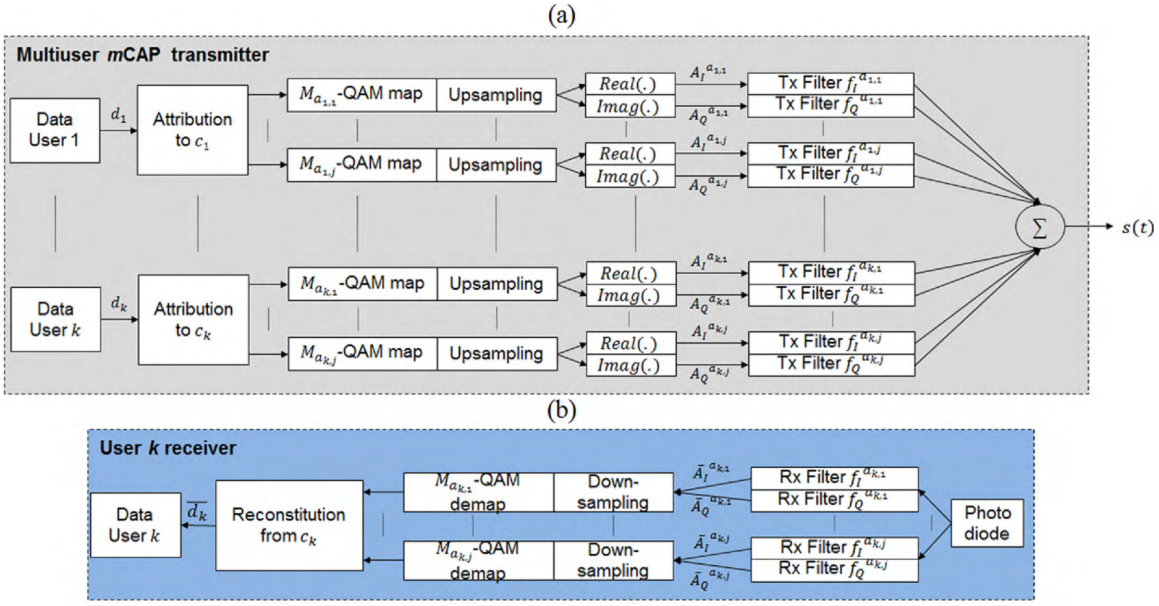

FIGURE 3. (a) Schematic representing the principle of a transmitter using SCM-based Multi-user Multi-band CAP (MU-mCAP) (b) Schematic representing the principle of a receiver using SCM-MU-mCAP.

Each pair of filter for the nth subcarrier is defined as follows:

$$rc(t) = \frac{\sin(\pi(1-\alpha)\frac{t}{T_s}) + 4\alpha\frac{t}{T_s}\cos(\pi(1-\alpha)\frac{t}{T_s})}{\pi\frac{t}{T_s}(1-(4\alpha\frac{t}{T_s})^2)} \quad (2)$$

$$f_I^n(t) = rc(t)\cos(\pi\frac{t}{T_s}(2n-1)(1+\alpha)p) \quad (3)$$

$$f_Q^n(t) = rc(t)\sin(\pi\frac{t}{T_s}(2n-1)(1+\alpha)p) \quad (4)$$

With:

- $\frac{1}{2T_s}(2n-1)(1+\alpha)$: center frequency of the nth band,
- T_s: symbol duration,
- α: roll-off factor,
- p: subcarrier spacing configuration factor.

Finally, the transmitted signal is defined with Eq. 5, where $*$ is a time-domain convolution:

$$s(t) = \sum_{n=1}^{m}\left[A_I^{c_k}(t) * f_I^{c_k}(t) - A_Q^{c_k}(t) * f_Q^{c_k}(t)\right] \quad (5)$$

Each component of the sum represents a subband that can be assigned to a user with SCM. At a typical receiver for user ik, the up-sampled in-phase and quadrature mapped symbols for each of the user's assigned subcarriers (c_k) are recovered using the matched transmission pulse shaping filters, as illustrated in Fig. 3 (b). The recovered data stream is obtained after combining the j de-mapped symbols streams.

The subcarrier spacing configuration factor p is used to configure the spacing between subbands and is added as a factor to the definition of the square root raised cosine filters pair. The value of the center frequency for each subcarrier is changed when p is adjusted. Initial value is 1 which corresponds to no subcarrier spacing, with $p \in]0{:}+\infty]$. It is important to note that when p increases, the signal bandwidth increases by the same factor as well.

III. EXPERIMENT SETUP

Fig. 4 shows the experiment setup that was used to obtain the experimental results presented in the sections 4 and 5.

A. TRANSMITTER DESCRIPTION

An Arbitrary Waveform Generator (AWG - AFG3252C) stores a total of m random bit streams. The streams are defined as groups. They form packets of data for each user k. The number of data streams assigned to each user depends on the given subcarriers allocation c_k for each user. Essentially, it means that a user k is allocated a packet of j (size of c_k) random bits streams. Each of these data streams is assigned to a subcarrier of the m-CAP modulation. For every user, an M-QAM mapper maps each of the data streams forming its packet. Thus, it creates multiple symbol streams. After up-sampling, a symbol stream is separated into its real and imaginary component. The corresponding in-phase and quadrature raised cosine filters are applied to them. These FIR filters are configured at the center frequency defined by the subcarrier assignation. All the m resulting modulated data streams are added to produce the signal s(t).

Before the transmission, the signal is pre-equalized using a software implemented amplitude pre-emphasis pre-equalization filter [39] to extend the available modulation bandwidth. In order to detect the transmitted frame at the receiver, a simple preamble is added at the beginning of the signal, before the transmission. The first part is a very low frequency waveform used by the receiver to detect the presence of a frame. The second part is a pilot in order to

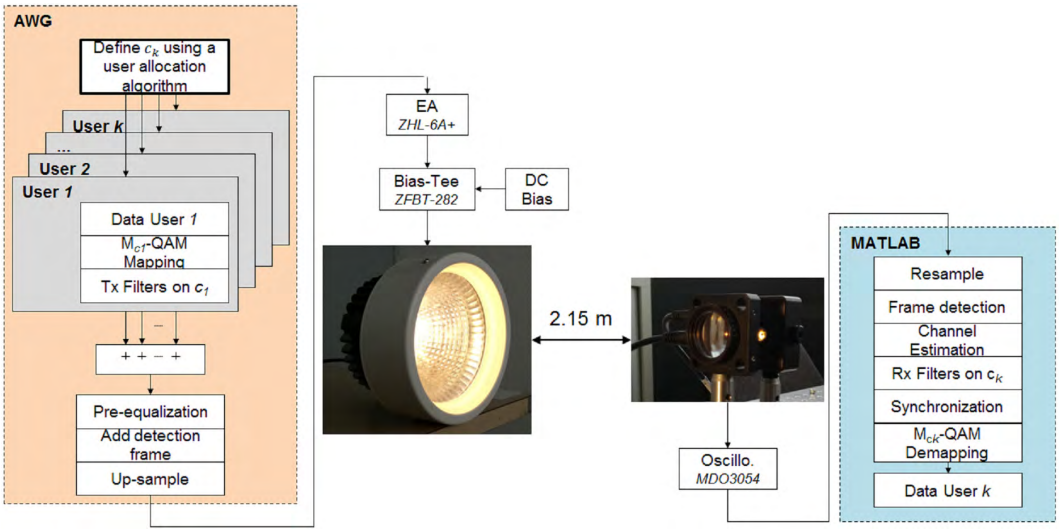

FIGURE 4. Schematic representing the experiment setup for the transmitter based on an AWG, an office downlight (top) and a receiver for a user k based on a photo-diode and an offline post-process with MATLAB (bottom).

identify the start of the signal. Also, it serves as a reference for the gain and phase corrections.

The AWG emits the signal. A Minicircuit electrical amplifier (ZHL-6A+) is used to amplify the signal outputted by the AWG. A Minicircuit bias-tee (ZFBT-282) adds a DC bias to the signal before sending it to the LED. The white LED used throughout the experiments is a 42 W downlight that can be found in malls, offices or hospitals. It operates at 19.2 W electrical power (32 V, 600 mA). Fig. 5 details the characteristics of the downlight used in this experimental system. The −3 dB modulation bandwidth is measured at 1.4 MHz.

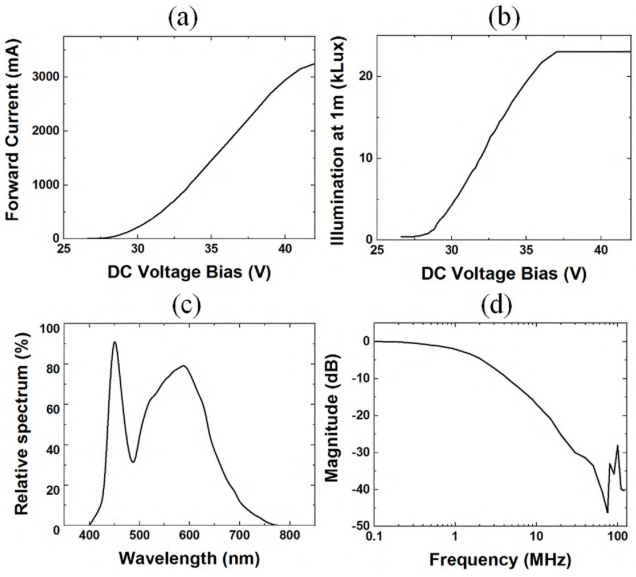

FIGURE 5. Experimental setup measured characteristics. (a) White LED current response versus voltage. (b) White LED illumination response versus voltage. (c) LED relative spectrum response versus wavelength. (d) Experimental system frequency response.

B. RECEIVER DESCRIPTION

A 25 mm biconvex lens and a Thorlabs photo-detector (PDA10A) form the receiver for a user k. The latter is composed of a 1 mm diameter silicon photo-diode and a trans-impedance amplifier circuit. The distance between the transmitter and a receiver is set at 2.15 m with line of sight (LOS) except when indicated otherwise. A receiver output signal is saved using a digital oscilloscope (MDO3054). The resulting data is post-processed using MATLAB. After re-sampling the signal, the preamble is decoded to identify the start of the signal that was sent. The matched filters deployed for demodulation depend on the allocation of subcarriers c_k for user k. The first subcarrier contains that information. Afterwards, the mapped symbols are corrected in gain and phase. Then, a decision feedback equalizer (DFE) performs a post-equalization. Lastly, they are de-mapped using the appropriate M-QAM demodulator. Thus, the packet of data sent to user k is obtained. Table 2 resumes the experiment setup and parameters.

TABLE 2. Experiment setup parameters and conditions.

Parameter	Value
Transmitter	42W white LED downlight
Receiver	150 MHz PDA10A-EC + 25 mm biconvex lens
-3dB bandwidth	1.4 MHz
Distance	2.15 m
DC Voltage bias	32 V
Forward current	600 mA
Illumination	10 klux
Raised cosine filter parameters	Roll-off = 0.15 Span = 12 Oversampling = 10

IV. OPTIMIZATION OF SPECTRAL EFFICIENCY IN MULTIBAND CAP

As explained in section 1, multiband CAP is a very recent modulation scheme in VLC. As such, there is a need to

explore its capabilities further. Indeed, the cited works presented the modulation or showed their effectiveness with heavy post-processing. Thus, our approach aims at improving the scheme in flexibility and data rate performances. To do so, low-complexity BER improvements are investigated. Subcarrier spacing is one of them. This allows for an improvement in the multi-user flexibility. Multi-access in VLC needs a lot of adaptability. For example, every person in an office room can potentially need different data in very different conditions: differences in angle of incidence, location on the Li-Fi cell or distance from the transmitter. Thus, exploring subcarrier spacing and other scheme performance improvements help us in our multi-users scenario.

Additionally, this work is constrained to a realistic scenario. Indeed, as explained in section 3, the distance between the transceivers is 2.15 meter and the LED is a low-cost commercial malls or offices downlight. The premises of low-complexity performances improvements for Multiband CAP were already described in [33]. This previous work showed the potential of using different filter parameters for each subcarrier. However, it had limitations as described in the introduction. Consequently, the possibilities given by the filter parameters are explored further in the following measurements.

A. SUBCARRIER SPACING

Multiband CAP uses pulse shaping filters that do not have a perfect rectangular frequency response and is therefore subject to inter-channel interferences (ICI). They reduce the quality of the received signal by adding noise on each adjacent subcarrier. Spacing the subbands would mitigate these interferences. The cost is an increase in bandwidth. In equations (2) and (3), the conventional definition of the square root raised cosine filter includes a factor p. This separate variable allows us to modify the subcarrier spacing by changing the center frequency of a filter, as shown in fig. 6. When spacing is increased, the signal bandwidth raises. Thus, the ICI decreases. However, the BER doesn't necessarily fall. Indeed, the wireless optical channel has a low-pass effect [40] and thus, an increase in bandwidth results in a decrease in signal-to-noise ratio (SNR). In our previous work [33], we concluded that this change in SNR affected the last subcarriers the most. As a consequence, the optimization needs to take this condition into consideration.

In the measures described in fig. 7, the effect of different subcarrier spacing configuration on the spectral efficiency is investigated. To measure it, the data rate is maximized in the condition of the experiment described section 3. The first configuration uses no subcarrier spacing. The second configuration uses the same spacing value between each subcarrier and is called uniform subcarrier spacing. The spacing value chosen maximizes the data rate. Lastly, the last configuration uses the best subcarrier spacing between each subcarrier and is called independent subcarrier spacing. These spacing values maximize the data rate.

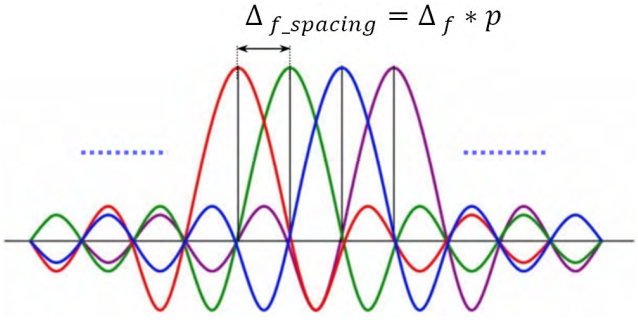

FIGURE 6. Multiband CAP filters responses and the impact of subcarrier spacing with the factor p. Δ_f is the frequency increment between each subband without spacing. $\Delta_{f_{spacing}}$ is the frequency increment between each subband with spacing.

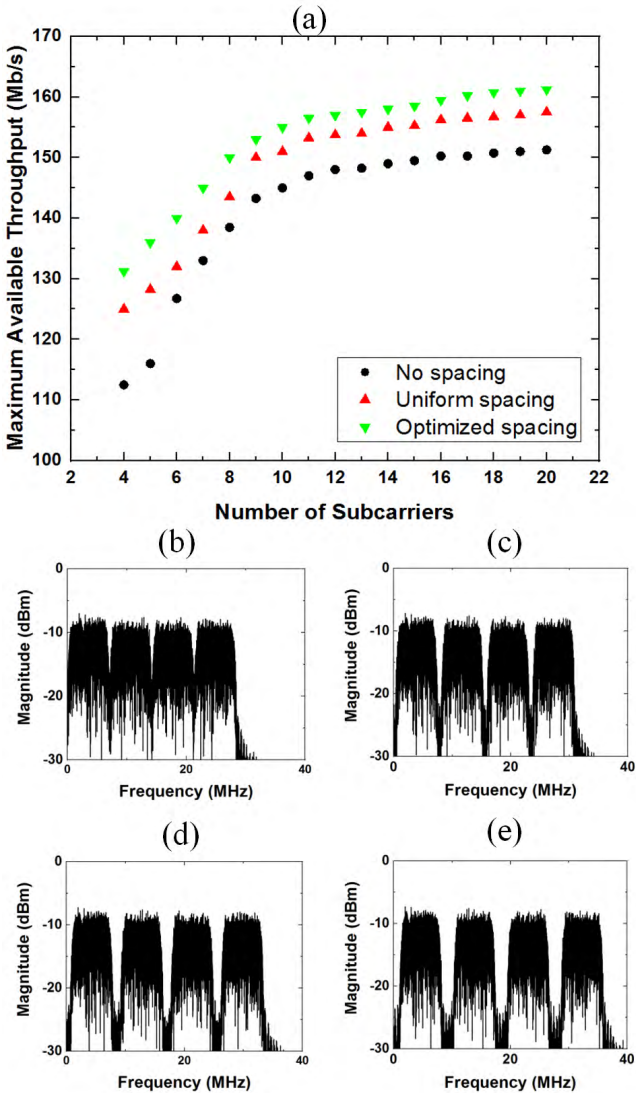

FIGURE 7. Measured impact of subcarrier spacing. (a) Obtained spectral efficiency while maximizing the data rate versus the number of subcarriers. The measurement are performed without spacing, with the same spacing value and with a spacing value optimized between each subband. Measured spectrum in a 4 subcarrier signal with no spacing (b), 5% spacing (c), 10% spacing (d), and 20% spacing (e).

The first observation is that an increase in the number of subcarriers results in an increase in performances. It already has been explored in the previous works on multiband CAP described in section 1. Indeed, we work out-of-band and thus the frequency response of the LED is not flat. With smaller subcarrier bandwidth, the associated response is more flat and thus the subband can use a higher modulation order.

With subcarrier spacing, the ICI has decreased, but the bandwidth of the signal increases. In turn, the SNR falls. With uniform spacing, the increase in performances for the first subcarriers compensate for the decrease in the last subcarriers. With optimized spacing, the first subcarriers have larger spacing ($> 10\%$) and the last ones have a smaller ($< 5\%$) to no spacing. The first subbands have a SNR high enough and the decrease in ICI is sufficient to use a higher modulation order. But, in order to not increase the signal bandwidth too much, the last subcarriers use an average spacing of 2.5 %. Thus, as shown in fig. 7, an increase in data rate of 16.6 % to 6.6 % is obtained with 4 to 20 subcarriers using optimized spacing while the values are 11.1 % to 4.13 % using uniform spacing. The difference is bigger when using a small number of subbands because the signal doesn't use an optimal amount of subcarriers. Indeed, as explained in the previous paragraph, when increasing the number of subcarriers, a higher modulation order can be used because the frequency response associated is more flat. As such, the margin for an increase in performances using subcarrier spacing only decreases. Consequently, other optimization methods are explored.

B. FLEXIBILITY AND PERFORMANCE OPTIMIZATIONS

More flexibility can be obtained with the optimization of the roll-off factor and oversampling [33]. Indeed, the higher the roll-off factor is, the larger the bandwidth is and the lower the non-linearity of the filter's response is. As such, when modifying all parameters at the same time, multiple scenarios with an increase in performances appear. That flexibility helps in a multi-users scenario where all receivers have very differents SNRs.

In order to explore this flexibility, the impact of the roll-off factor on the data rate is compared with the results obtained in the previous subsection. With no spacing, and the same parameters, each subcarrier has a roll-off value optimized in order to maximize the total data rate. Then, subcarrier spacing is associated with roll-off factor in the optimization. The process to obtain the parameters for all subcarriers is described fig. 8. As the subject of this work focuses on the results of the optimization and not the method, a conventional loop algorithm is used in two steps. The first one is a uniform optimization where the same global value for either of the parameter is set for all subcarrier. The objective is to obtain the value of subcarrier spacing and roll-off factor which minimize the BER, p_U and α_U respectively. The second step of the algorithm is once again a conventional loop which finds the optimal value for p and α. The results are compiled in fig. 9 (a), adding intermediary results where only the roll-off factor or only the subcarrier spacing factor is optimized.

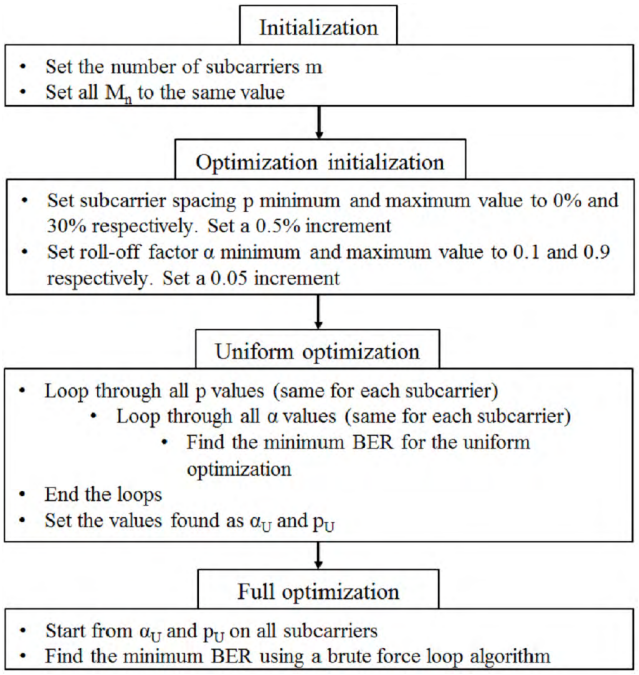

FIGURE 8. Optimization process pseudo-code for obtaining the optimized filter parameters in both the uniform optimization and the full optimization process.

Fig. 9 (b) and (c) show the individual impact of the roll-off factor and subcarrier spacing on each subcarrier of a 4-CAP signal.

The roll-off factor impact is shown fig. 9 (b). The higher the value, the less clipping the subband filter will experience. Its bandwidth will also increase. As such, the first subcarriers offer better performances with a larger roll-off factor. Thus, when optimizing the parameter, the optimal value for each subcarrier decreases with the subband index. As shown in fig. 9 (a), an increase in data rate of 11.11 % to 4.13 % is obtained for 4 to 20 subcarriers. When associating the optimization of the roll-off factor with subcarrier spacing, a boost in data rate of 27.78 % to 7.44 % is attained for 4 to 20 subcarriers. At 20 subcarriers, this is equal to an addition of 11.25 Mb/s. Indeed, the full optimization offers more degree of liberty and thus more scenarios with an increase in data rate are observed. A large roll-off factor increases the bandwidth of the subcarrier associated. In return, it augments the interferences between subbands. But, with subcarrier spacing, we can reduce these interferences. As such, the full optimization attains larger increase in data rate.

The enhancement in performance is higher at lower number of subcarriers. Indeed, a relative augmentation of 11.1% is observed for the roll-off factor only optimization, 16.67% for the subcarrier only one and 27.78% for the full process in a 4 subbands scenario. When using a 20 subcarriers signal, these numbers go down to 4.13%, 6.61% and 7.44% respectively. When subbands have a larger bandwidth, the effect of the low-pass distortion is stronger on them. However, adverse effects are prominent on the first few parts of the signal

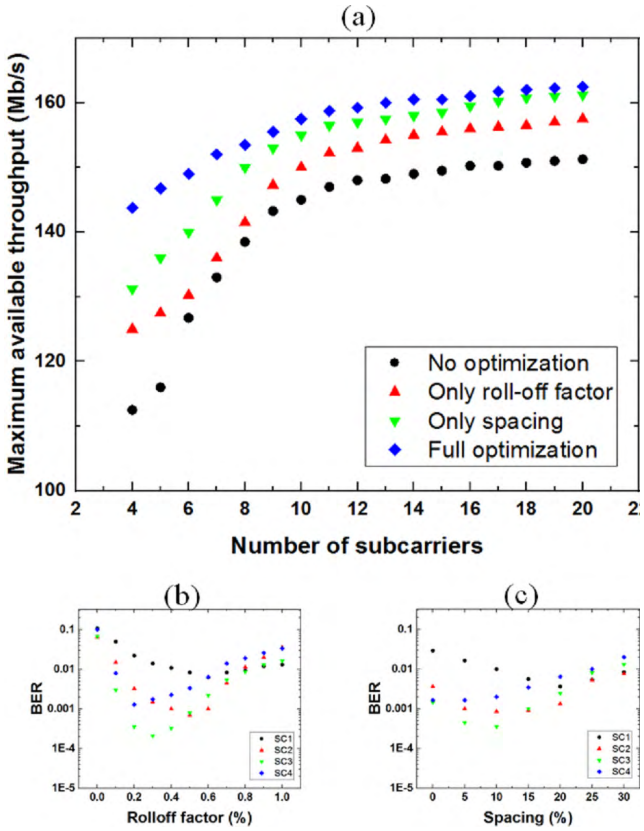

FIGURE 9. (a) Change in data rate performances compared to no filter parameter optimization on our experimental setup. Optimization is performed on spacing, roll-off or both. (b) Impact of the roll-off factor on each subcarrier BER. (c) Impact of subcarrier spacing on each subcarrier data rate.

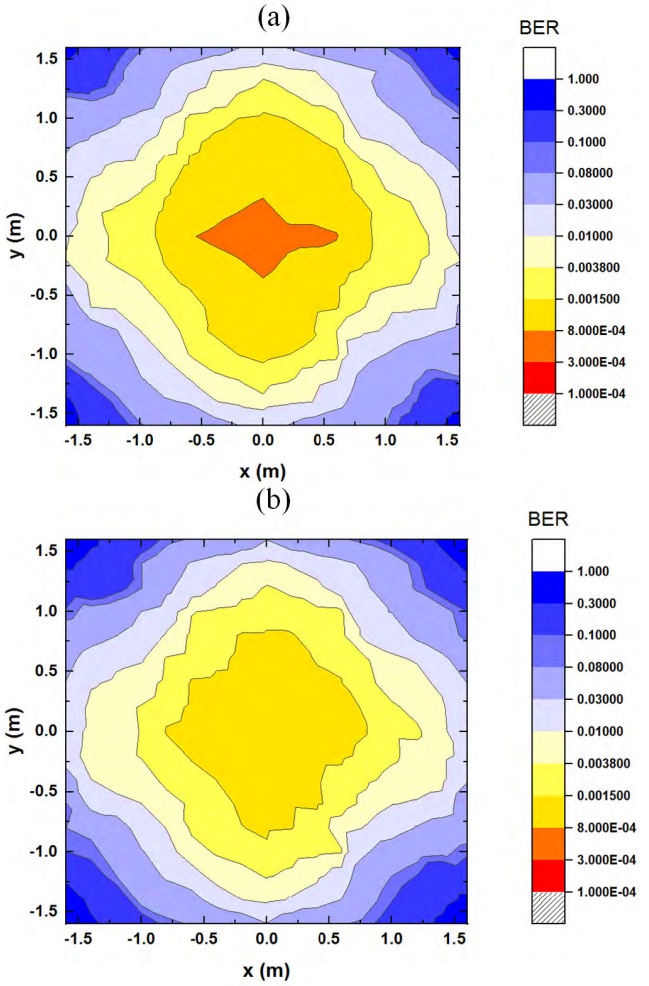

FIGURE 10. BER measured on a 2D plane situated 2.15 meter away from the transmitter, with performance optimization (a) and without (b).

bandwidth for clipping noise and the last parts for the Gaussian noise. With 4 subcarriers, a localized effect impacts a fourth of the total frame while it only effects one twentieth when 20 subcarriers are used. Essentially, multiband CAP signals with higher total number of subbands have less headroom for data rate improvements. However, the BER can still be reduced on all subcarriers even if not enough for an increase in throughput. The BER on the receiving plane can thus be improved and expands the size of the attocell, as described in the following subsection.

C. BER PERFORMANCES IN THE ATTOCELL

In a multi-users scenario, each user will be spread randomly in the VLC attocell. Thus, we need to understand the impact of the performance optimizations explored in the previous subsection on the potential location of a user in the attocell. The BER obtained on a 2D plane situated 2.15 meter away from the transmitter is measured without performance optimization and with performance optimization. The results are shown in fig. 10. Thus, the size of the attocell is compared in the two scenarios.

The results show that a cell size of approximately 3.2 meter square is obtained without the optimization and 4.56 meter square with optimization. The size is defined as the area where the BER for each subcarrier is below 3.8×10-3. This is the forward error correction (FEC) 7% value. This means that this percentage in the raw data rate can be used to correct the whole signal with FEC pre-coding.

Our previous results described in fig. 9 help depicting the effect. Indeed, subcarrier number 20 sees a decrease in BER to 8.47×10^{-3} from 1.03×10^{-3} with a 16-QAM constellation when a full optimization is applied. This decrease in BER does not allow for an augmentation of the modulation order, as verified by our measurements since using a 32-QAM constellation resulted in a 4.17×10^{-3} bit error rate. This is slightly above the 7% FEC limit. Overall, this scenario occurs more often on higher subband count since, as explained in the previous subsection, the headroom for improvement is smaller, as per our measurements. The BER plane measurements shown fig. 10 were performed with a 20-CAP signal. Thus, both attocells are the same except that when using applying a full optimization, the BER is overall decreased which means that a small part of the outer border now falls under the 7% FEC threshold.

TABLE 3. Multi-user signal characteristics and results in a 4 users scenario.

Parameter	Value	
Number of subcarriers	20	
User capacity	1 to 20 users	
Subcarrier spacing	{30, 25, 20, 20, 20, 15, 10, 10, 7.5, 5, 2.5, 1, 0, 0, 0}	
Roll-off factor	{0.7, 0.6, 0.6, 0.6, 0.5, 0.5, 0.5, 0.4, 0.4, 0.4, 0.4, 0.3, 0.3, 0.2, 0.2, 0.2, 0.15, 0.15, 0.15, 0.15}	
Constellation size	M = {32, 64, 128, 128, 256, 256, 128, 128, 128, 128, 128, 128, 64, 64, 64, 64, 64, 64, 16}	
Distance	2.15 m	
Total throughput	162.5 Mb/s	
Signal bandwidth	32 MHz	
User 1	c_1 = {1, 4, 7, 12, 19}	40 Mb/s
User 2	c_2 = {3, 8, 13, 15, 20}	38.75 Mb/s
User 3	c_3 = {2, 10, 11, 14, 17}	40 Mb/s
User 4	c_4 = {5, 6, 9, 16, 18}	43.75 Mb/s

V. SYNTHESIS OF THE OVERALL SYSTEM

Table 3 resumes the characteristics of the experimental setup. The results described in the previous section help us optimize the performances in spectral efficiency. Fig. 11 shows the signal spectrum measured received by a user at 2.15 meter of distance from the transmitter. In this 4-users scenario, subcarrier allocation is realized before the emission of the signal. Here, a static allocation is utilized. Each user must attain the same data rate, or as close as possible. Twenty subcarriers are used in the signal since it provides a capacity of 20 users or the ability to allocate multiple subbands per users. Therefore, five subcarriers are allocated to each user in this 4-users example. This lessens the impact of a loss of quality on one subband. A minor part of the data carried by the first subcarrier contains the allocation that each user reads before decoding the appropriate subbands. Finally, each user must experience a comparable BER. Since there's no up-link, the center frequency of the subcarriers allocated to a user is at the center of the signal bandwidth. This explains the way the allocation is performed as shown in fig. 11.

Using SCM, the number of subcarriers is the number of users that can be allocated. With 20 subbands in our case, a total of 20 users could be served with one subcarrier per user. However, scalability is an issue. Indeed, the signal is optimized for data rate. As shown in table 3, most subcarriers do not operate at the same modulation order. As an example, if 20 users are allocated in our experiment setup, a user being allocated subcarrier 20 will receive data at a rate of 5 Mb/s while a user being designated subcarrier 5 will acquire data at a rate of 10 Mb/s. While this is the most extreme scenario in our case, it shows that scalability in terms of data rate per user is an issue in this VLC system. Dynamic subcarrier allocation would help alleviate this escalating problem. Our previous work discussed in [41] speaks of this exact method. Results show that when defining a target data rate for each user, only a certain amount of receivers can be allocated while maintaining their data rate within 5% of their target. However, a VLC attocell is small and will most likely not serve such a large number of users. This is the reason why we consider the dynamic subcarrier allocation scheme to help improve flexibility more than alleviating the scalability issue. Essentially, the same number of users is allocated up to their target data rate using an optimal allocation algorithm. Therefore, more headroom is obtained in the form of available subcarriers.

Fig. 12 shows the three dimensional BER measured under the conditions described section III and table 3. The attocell has a surface of 4.56 m^2. This corresponds to the area where the BER is low enough to be corrected by a Forward Error Correction (FEC) pre-coding. It represents the results

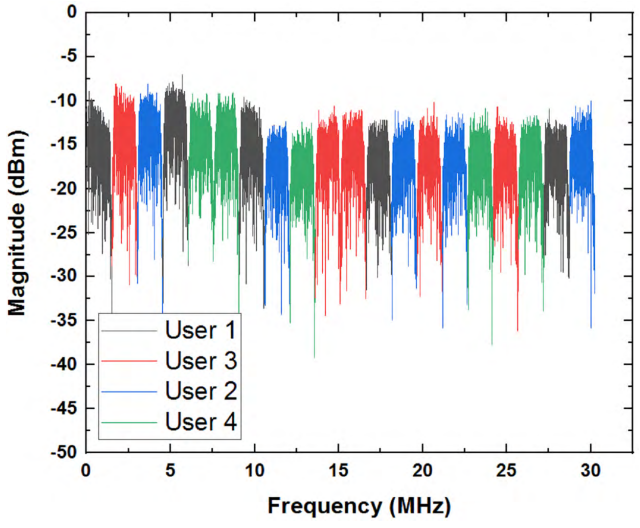

FIGURE 11. Signal spectrum measured at the receiver at 2.15 meter distance from the transmitter in a 4-users scenario. In this static allocation, a user will only decode the data contained in its assigned subcarriers.

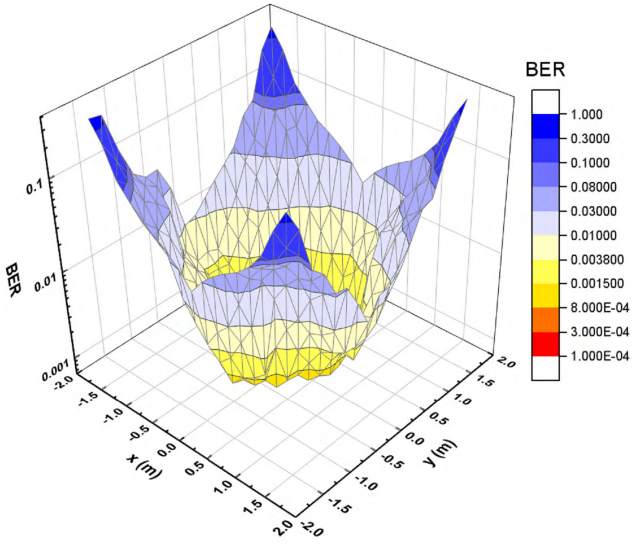

FIGURE 12. Measured three-dimensional BER with the receiver positioned at 2.15 meter away from the downlight LED transmitter.

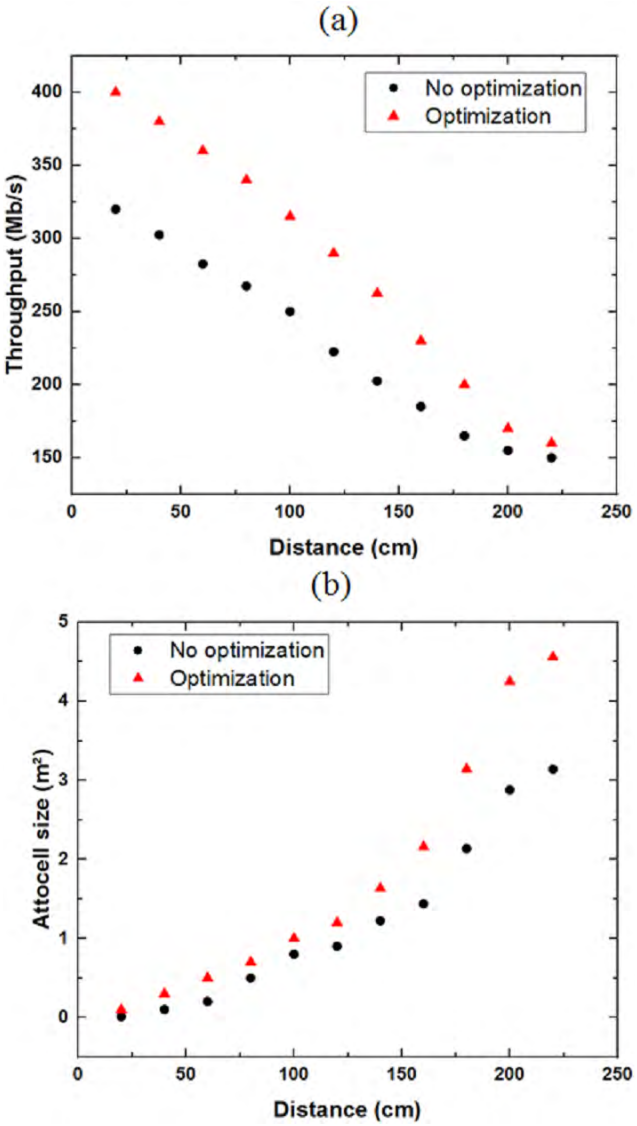

FIGURE 13. Maximum available throughput (a) and size of the attocell (b) versus the distance between the transmitter and receiver placed in direct line of sight. The measures are obtained with and without the performance optimization.

obtained in the previous subsection but do a better job showcasing the progression of the quality of service throughout the receiving plane. The BER value must be under $3.8\times10\text{-}3$. The cell total capacity is 34 Mb/s/m^2 and has the ability to serve up to 20 users simultaneously at an average rate of 8 Mb/s. Since the cell is small, a more relevant value is the mean throughput of 40 to 80 Mb/s/user in a 2 to 4 users scenario. Finally, fig. 13 shows the measured influence of the distance on the maximum available throughput and the size of the cell. As expected, data rate increases while the attocell size decreases when reducing the distance.

VI. CONCLUSION

The data rate is optimized with little computational work. Indeed, using the optimization of subcarrier filters parameters, an increase in throughput is achieved. The setup successfully attained a 5.08 b/s/Hz spectral efficiency while maximizing the total data rate. A simple post-equalization scheme was the only addition to the process. In conclusion, multiband CAP associated with SCM proves to be a compelling alternative scheme for high spectral efficiency VLC systems in multi-users scenarios. The performances obtained can fit a realistic indoor scenario, with a capacity of 1 to 20 users and high data rate in a relatively large attocell.

VII. PERSPECTIVES

This work will serve as a basis for further exploration through its implementation in a real-time system with a field-programmable gate array (FPGA). This will allow us to compare the performances of the very popular OFDM with m-CAP in the same scenario as in this paper. We can also identify a compromise between throughput and cost of implementation.

REFERENCES

[1] H. Elgala, R. Mesleh, and H. Haas, "Indoor optical wireless communication: Potential and state-of-the-art," *IEEE Commun. Mag.*, vol. 49, no. 9, pp. 56–62, Sep. 2011, doi: 10.1109/MCOM.2011.6011734.

[2] H. Haas, L. Yin, Y. Wang, and C. Chen, "What is LiFi?" *J. Lightw. Technol.*, vol. 34, no. 6, pp. 1533–1544, Mar. 15, 2016, doi: 10.1109/JLT.2015.2510021.

[3] B. Béchadergue, L. Chassagne, and H. Guan, "Experimental comparison of pulse-amplitude and spatial modulations for vehicle-to-vehicle visible light communication in platoon configurations," *Opt. Express*, vol. 25, no. 20, pp. 24790–24802, 2017.

[4] J. Armstrong, Y. A. Sekercioglu, and A. Neild, "Visible light positioning: A roadmap for international standardization," *IEEE Commun. Mag.*, vol. 51, no. 12, pp. 68–73, Dec. 2013, doi: 10.1109/MCOM.2013.6685759.

[5] P. H. Pathak, X. Feng, P. Hu, and P. Mohapatra, "Visible light communication, networking, and sensing: A survey, potential and challenges," *IEEE Commun. Surveys Tuts.*, vol. 17, no. 4, pp. 2047–2077, 4th Quart., 2015, doi: 10.1109/COMST.2015.2476474.

[6] Y. Zhou, J. Zhao, M. Zhang, J. Shi, and N. Chi, "2.32 Gbit/s phosphorescent white LED visible light communication aided by two-staged linear software equalizer," *Proc. 10th Int. Symp. Commun. Syst., Netw. Digit. Signal Process. (CSNDSP), Prague*, 2016, pp. 1–4, doi: 10.1109/CSNDSP.2016.7573913.

[7] Y. Zhou, S. Liang, S. Chen, X. Huang, and N. Chi, "2.08 Gbit/s visible light communication utilizing power exponential pre-equalization," in *Proc. 25th Wireless Opt. Commun. Conf. (WOCC)*, Chengdu, China, May 2016, pp. 1–3.

[8] D. Karunatilaka, F. Zafar, V. Kalavally, and R. Parthiban, "LED based indoor visible light communications: State of the art," *IEEE Commun. Surveys Tuts.*, vol. 17, no. 3, pp. 1649–1678, 3rd Quart., 2015, doi: 10.1109/COMST.2015.2417576.

[9] F. M. Wu *et al.*, "Performance comparison of OFDM signal and CAP signal over high capacity RGB-LED-based WDM visible light communication," *IEEE Photon. J.*, vol. 5, no. 4, Aug. 2013, Art. no. 7901507, doi: 10.1109/JPHOT.2013.2271637.

[10] M. I. Olmedo *et al.*, "Multiband carrierless amplitude phase modulation for high capacity optical data links," *J. Lightw. Technol.*, vol. 32, no. 4, pp. 798–804, Feb. 15, 2014, doi: 10.1109/JLT.2013.2284926.

[11] J. Wei, Q. Cheng, D. G. Cunningham, R. V. Penty, and I. H. White, "100-Gb/s hybrid multiband CAP/QAM signal transmission over a single wavelength," *J. Lightw. Technol.*, vol. 33, no. 2, pp. 415–423, Jan. 15, 2015, doi: 10.1109/JLT.2014.2387352.

[12] M. Xu *et al.*, "Orthogonal multiband CAP modulation based on offset-QAM and advanced filter design in spectral efficient MMW RoF systems," *J. Lightw. Technol.*, vol. 35, no. 4, pp. 997–1005, Feb. 15, 2017, doi: 10.1109/JLT.2016.2593443.

[13] P. A. Haigh *et al.*, "A multi-CAP visible-light communications system with 4.85-b/s/Hz spectral efficiency," *IEEE J. Sel. Areas Commun.*, vol. 33, no. 9, pp. 1771–1779, Sep. 2015, doi: 10.1109/JSAC.2015.2433053.

[14] P. Chvojka *et al.*, "On the m-CAP performance with different pulse shaping filters parameters for visible light communications," *IEEE Photon. J.*, vol. 9, no. 5, Oct. 2017, Art. no. 7906712, doi: 10.1109/JPHOT.2017.2749203.

[15] K. Werfli *et al.*, "Multi-band carrier-less amplitude and phase modulation with decision feedback equalization for bandlimited VLC systems," in *Proc. 4th Int. Workshop Opt. Wireless Commun. (IWOW)*, Istanbul, Turkey, Sep. 2015, pp. 6–10, doi: 10.1109/IWOW.2015.7342255.

[16] K. Werfli *et al.*, "Experimental demonstration of high-speed 4×4 imaging multi-CAP MIMO visible light communications," *J. Lightw. Technol.*, vol. 36, no. 10, pp. 1944–1951, May 15, 2018.

[17] Y. Wang, L. Tao, Y. Wang, and N. Chi, "High speed WDM VLC system based on multi-band CAP64 with weighted pre-equalization and modified CMMA based post-equalization," *IEEE Commun. Lett.*, vol. 18, no. 10, pp. 1719–1722, Oct. 2014, doi: 10.1109/LCOMM.2014.2349990.

[18] X. Lu, K. Wang, L. Qiao, W. Zhou, Y. Wang, and N. Chi, "Nonlinear compensation of multi-CAP VLC system employing clustering algorithm based perception decision," *IEEE Photon. J.*, vol. 9, no. 5, Oct. 2017, Art. no. 7906509, doi: 10.1109/JPHOT.2017.2748153.

[19] X. Huang, F. Yang, and J. Song, "Novel heterogeneous attocell network based on the enhanced ADO-OFDM for VLC," *IEEE Commun. Lett.*, vol. 23, no. 1, pp. 40–43, Jan. 2019, doi: 10.1109/LCOMM.2018.2880200.

[20] H. Ma, L. Lampe, and S. Hranilovic, "Coordinated broadcasting for multiuser indoor visible light communication systems," *IEEE Trans. Commun.*, vol. 63, no. 9, pp. 3313–3324, Sep. 2015, doi: 10.1109/TCOMM.2015.2452254.

[21] H. Kazemi, M. Safari, and H. Haas, "A wireless backhaul solution using visible light communication for indoor Li-Fi attocell networks," in *Proc. IEEE Int. Conf. Commun. (ICC)*, Paris, France, May 2017, pp. 1–7, doi: 10.1109/ICC.2017.7996637.

[22] H. Alshaer and H. Haas, "Bidirectional LiFi attocell access point slicing scheme," *IEEE Trans. Netw. Service Manage.*, vol. 15, no. 3, pp. 909–922, Sep. 2018, doi: 10.1109/TNSM.2018.2842055.

[23] Z. Li and C. Zhang, "A novel VLC attocell network structure using superimposed optical-OFDM," in *Proc. 14th Int. Wireless Commun. Mobile Comput. Conf. (IWCMC)*, Limassol, Cyprus, 2018, pp. 642–647, doi: 10.1109/IWCMC.2018.8450307.

[24] J.-Y. Sung, C.-H. Yeh, C.-W. Chow, W.-F. Lin, and Y. Liu, "Orthogonal frequency-division multiplexing access (OFDMA) based wireless visible light communication (VLC) system," *Opt. Commun.*, vol. 355, pp. 261–268, Nov. 2015, doi: 10.1016/j.optcom.2015.06.070.

[25] C. Yang, Y. Wang, Y. Wang, X. Huang, and N. Chi, "Demonstration of high-speed multi-user multi-carrier CDMA visible light communication," *Opt. Commun.*, vol. 336, pp. 269–272, Feb. 2015, doi: 10.1016/j.optcom.2014.09.072.

[26] Z. Chen and H. Haas, "Space division multiple access in visible light communications," in *Proc. IEEE Int. Conf. Commun. (ICC)*, London, U.K., Jun. 2015, pp. 5115–5119, doi: 10.1109/ICC.2015.7249135.

[27] Z. Yu, R. J. Baxley, and G. T. Zhou, "Multi-user MISO broadcasting for indoor visible light communication," in *Proc. IEEE Int. Conf. Acoust., Speech Signal Process.*, Vancouver, BC, USA, May 2013, pp. 4849–4853, doi: 10.1109/ICASSP.2013.6638582.

[28] L. Dai, B. Wang, Y. Yuan, S. Han, C.-L. I, and Z. Wang, "Non-orthogonal multiple access for 5G: Solutions, challenges, opportunities, and future research trends," *IEEE Commun. Mag.*, vol. 53, no. 9, pp. 74–81, Sep. 2015. doi: 10.1109/MCOM.2015.7263349.

[29] L. Yin, W. O. Popoola, X. Wu, and H. Haas, "Performance evaluation of non-orthogonal multiple access in visible light communication," *IEEE Trans. Commun.*, vol. 64, no. 12, pp. 5162–5175, Dec. 2016, doi: 10.1109/TCOMM.2016.2612195.

[30] B. Lin, W. Ye, X. Tang, and Z. Ghassemlooy, "Experimental demonstration of bidirectional NOMA-OFDMA visible light communications," *Opt. Express*, vol. 25, no. 4, pp. 4348–4355, 2017, doi: 10.1364/OE.25.004348.

[31] C. Chen, W. Zhong, H. Yang, P. Du, and Y. Yang, "Flexible-rate SIC-free NOMA for downlink VLC based on constellation partitioning coding," *IEEE Wireless Commun. Lett.*, to be published. [Online]. Available: https://ieeexplore.ieee.org/document/8527543, doi: 10.1109/LWC.2018.2879924.

[32] C.-H. Lee, W. V. Sorin, and B. Y. Kim, "Fiber to the home using a PON infrastructure," *J. Lightw. Technol.*, vol. 24, no. 12, pp. 4568–4583, Dec. 2006, doi: 10.1109/JLT.2006.885779.

[33] M. M. Merah, H. Guan, and L. Chassagne, "Performance optimization in multi-user multiband carrierless amplitude and phase modulation for visible light communication," in *Proc. Global LIFI Congress (GLC)*, Paris, France, Feb. 2018, pp. 1–4, doi: 10.23919/GLC.2018.8319114.

[34] B. Wilson, Z. Ghassemlooy, and I. Darwazeh, *Analogue Optical Fibre Communications* (Telecommunications). Edison, NJ, USA: IET, 1995, [Online]. Available: http://digital-library.theiet.org/content/books/te/pbte032e

[35] T. Komine, S. Haruyama, and M. Nakagawa, "Bi-directional visible-light communication using corner cube modulator," in *Proc. IASTED Int. Conf. Wireless Opt. Commun.*, vol. 3, L. Hesselink, Ed., 2003, pp. 598–603.

[36] X. Jin, B. A. Hristovski, C. M. Collier, S. Geoffroy-Gagnon, B. Born, and J. Holzman, "Spherical transceivers for ultrafast optical wireless communications," *Proc. SPIE*, vol. 9744, p. 97440F, Feb. 2016, doi: 10.1117/12.2208343.

[37] M. Vladescu and D. T. Vuza, "Redundant uplink optical channel for visible light communication systems," *Proc. SPIE*, vol. 9258, p. 92581J, Feb. 2015.

[38] K. Cui, G. Chen, Q. He, and Z. Xu, "Indoor optical wireless communication by ultraviolet and visible light," *Proc. SPIE*, vol. 7464, Aug. 2009, Art. no. 74640D.

[39] X. Huang, J. Shi, J. Li, Y. Wang, Y. Wang, and N. Chi, "750 Mbit/s visible light communications employing 64QAM-OFDM based on amplitude equalization circuit," in *Proc. Opt. Fiber Commun. Conf. Exhib. (OFC)*, Los Angeles, CA, USA, Mar. 2015, pp. 1–3.

[40] Z. Wang, Q. Wang, W. Huang, and Z. Xu, "Visible light communications: Channel and capacity," in *Visible Light Communications: Modulation and Signal Processing*, vol. 1. Hoboken, NJ, USA: Wiley, 2018, p. 368, doi: 10.1002/9781119331865.

[41] M. M. Merah, L. Chassagne, and H. Guan, "Experimental demonstration of user allocation in a subcarrier multiplexing-based multiuser LiFi system," in *Proc. IEEE Photon. Conf. (IPC)*, Reston, VA, USA, Sep./Oct. 2018, pp. 1–2, doi: 10.1109/IPCon.2018.8527235.

[42] Y. Wang, L. Tao, X. Huang, J. Shi, and N. Chi, "8-Gb/s RGBY LED-based WDM VLC system employing high-order CAP modulation and hybrid post equalizer," *IEEE Photon. J.*, vol. 7, no. 6, pp. 1–7, Dec. 2015.

[43] F.-M. Wu, C.-T. Lin, C.-C. Wei, C.-W. Chen, Z.-Y. Chen, and H.-T. Huang, "3.22-Gb/s WDM visible light communication of a single RGB LED employing carrier-less amplitude and phase modulation," in *Proc. Opt. Fiber Commun. Conf. Expo. Nat. Fiber Eng. Conf. (OFC/NFOEC)*, Anaheim, CA, USA, Mar. 2013, pp. 1–3.

[44] Y. Wang, X. Huang, L. Tao, J. Shi, and N. Chi, "4.5-Gb/s RGB-LED based WDM visible light communication system employing CAP modulation and RLS based adaptive equalization," *Opt. Express*, vol. 23, no. 10, pp. 13626–13633, 2015.

[45] D. Tsonev *et al.*, "A 3-Gb/s single-LED OFDM-based wireless VLC link using a gallium nitride μLED," *IEEE Photon. Technol. Lett.*, vol. 26, no. 7, pp. 637–640, Apr. 2014.

[46] C. L. Tsai, Y. C. Lu, and S. C. Ko, "Resonant-cavity light-emitting diodes (RCLEDs) made from a simple dielectric coating of transistor outline (TO)-can packaged InGaN LEDs for visible light communications," *IEEE Trans. Electron Devices*, vol. 63, no. 7, pp. 2802–2806, Jul. 2016.

[47] S. Rajbhandari *et al.*, "High-speed integrated visible light communication system: Device constraints and design considerations," *IEEE J. Sel. Areas Commun.*, vol. 33, no. 9, pp. 1750–1757, Sep. 2015.

[48] I.-C. Lu, Y.-L. Liu, and C.-H. Lai, "High-speed 2×2 MIMO-OFDM visible light communication employing phosphorescent LED," in *Proc. 8th Int. Conf. Ubiquitous Future Netw. (ICUFN)*, Vienna, Austria, Jul. 2016, pp. 222–224.

[49] H. Li *et al.*, "682 Mbit/s phosphorescent white LED visible light communications utilizing analog equalized 16QAM-OFDM modulation without blue filter," *Opt. Commun.*, vol. 354, pp. 107–111, Nov. 2015.

[50] G. Cossu, A. M. Khalid, P. Choudhury, R. Corsini, and E. Ciaramella, "3.4 Gbit/s visible optical wireless transmission based on RGB LED," *Opt. Express*, vol. 20, no. 26, pp. B501–B506, 2012.

[51] Q. Chen *et al.*, "Experimental research on adaptive 128/64QAM DFT-spread IFFT/FFT size efficient OFDM with a high SE in VLLC system," *IEEE Photon. J.*, vol. 9, no. 1, Feb. 2017, Art. no. 7900408.

[52] M. Shi, C. Wang, H. Guo, Y. Wang, X. Li, and N. Chi, "A high-speed visible light communication system based on DFT-S OFDM," in *Proc. IEEE Int. Conf. Commun. Syst. (ICCS)*, Shenzhen, China, Dec. 2016, pp. 1–5.

[53] R. Chen, K.-H. Park, C. Shen, T. K. Ng, B. S. Ooi, and M.-S. Alouini, "Visible light communication using DC-biased optical filter bank multi-carrier modulation," in *Proc. Global LIFI Congress (GLC)*, Paris, France, Feb. 2018, pp. 1–6.
[54] C. Yang, W. Liu, X. Li, Q. Yang, and Z. He, "Nyquist-PAM-4 transmission using linear DPD and MLSE for indoor visible light communications," in *Proc. IEEE/CIC Int. Conf. Commun. China (ICCC)*, Qingdao, China, Oct. 2017, pp. 1–2.
[55] Y. Hong, L.-K. Chen, and J. Zhao, "Experimental demonstration of performance-enhanced MIMO-OFDM visible light communications," in *Proc. Opt. Fiber Commun. Conf. Exhib. (OFC)*, Los Angeles, CA, USA, Mar. 2017, pp. 1–3.
[56] R. Bian *et al.*, "Experimental demonstration of generalised space shift keying for visible light communication," in *Proc. IEEE Int. Black Sea Conf. Commun. Netw. (BlackSeaCom)*, Istanbul, Turkey, Jun. 2017, pp. 1–5.

MOUNIR MOHAMMEDI MERAH received the B.S. degree in mathematics from Université Paris 13, Paris, France, in 2013, the M.S. degree in electrical engineering from INSA Lyon, Lyon, France, in 2016, and the M.S. degree in embedded systems from Université Claude Bernard, Lyon, in 2016. He is currently pursuing the Ph.D. degree in communication networks with the Université de Versailles Saint-Quentin, Versailles, France.

In 2016, he was a Research Intern with the CEA Nano-Innov, Palaiseau, France. His research interests include the development of wireless communicating networks and the study of visible light communication systems.

HONGYU GUAN received the B.S. degree in electrical engineering from ENSEIRB, France, in 2007, and the Ph.D. degree in computer science from the University of Bordeaux I, Bordeaux, France, in 2012, for his work on embedded systems for home automation. He is currently a Research Associate and the Chief Project Engineer with the LISV laboratory, Versailles Saint-Quentin-en-Yvelines University, University of Paris-Saclay.

His current research interests include visible light communications, communication protocol, ubiquitous, data fusion, sensors, and nanometrology.

LUC CHASSAGNE received the Engineer degree from Supélec, France, in 1994, and the Ph.D. degree in optoelectronics from the University of Paris XI, Orsay, France, in 2000, for his work in the field of atomic frequency standard metrology. He is currently a Professor and the Director of the LISV Laboratory, University of Paris-Saclay.

His research interests include nanometrology, precision displacements, sensors, and AFM instrumentation.